

# Symplectic map description of Halley's comet dynamics

G. Rollin, P. Haag, J. Lages

*Institut UTINAM, Observatoire des Sciences de l'Univers THETA, CNRS, Université de Franche-Comté, 25030  
Besançon, France*

---

## Abstract

We determine the two-dimensional symplectic map describing 1P/Halley chaotic dynamics. We compute the Solar system kick function ie the energy transfer to 1P/Halley along one passage through the Solar system. Each planet contribution to the Solar system kick function appears to be the sum of a Keplerian potential and of a rotating gravitational dipole potential due to the Sun movement around Solar system barycenter. The Halley map gives a reliable description of comet dynamics on time scales of  $10^4$ yr while on a larger scales the parameters of the map are slowly changing due to slow oscillations of orbital momentum.

---

## 1. Introduction

The short term regularity of 1P/Halley appearances in the Solar system (SS) contrasts with its long term irregular and unpredictable orbital behavior governed by dynamical chaos [1]. Such chaotic trajectories can be described by a Kepler map [1, 2] which is a two dimensional area preserving map involving energy and time. The Kepler map was originally analytically derived in the framework of the two dimensional restricted three body problem [2] and numerically constructed for the three dimensional realistic case of 1P/Halley [1]. Then the Kepler map has been used to study nearly parabolic comets with perihelion beyond Jupiter orbital radius [2–5], 1P/Halley chaotic dynamics [1, 6], mean motion resonances with primaries [7, 8], chaotic diffusion of comet trajectories [7, 9–12] and chaotic capture of dark matter by the SS and galaxies [13–15]. Alongside its application in celestial dynamics and astrophysics the Kepler map has been also used to describe atomic physics phenomena such as mi-

crowave ionization of excited hydrogen atoms [16–18], and chaotic autoionization of molecular Rydberg states [19].

In this work we semi-analytically determine the symplectic map describing 1P/Halley dynamics taking into account the Sun and the eight major planets of the SS. We use Melnikov integral (see *eg* [4, 20–24]) to compute exactly the kick functions associated to each major planet and in particular we retrieve the kick functions of Jupiter and Saturn which were already numerically extracted by Fourier analysis [1] from previously observed and computed 1P/Halley perihelion passages [25]. We show that each planet contribution to the SS kick function can be split into a Keplerian potential term and a rotating dipole potential term due to the Sun movement around SS barycenter. We illustrate the chaotic dynamics of 1P/Halley with the help of the symplectic Halley map and give an estimate of the 1P/Halley sojourn time. Then we discuss its long term robustness comparing the semi-analytically computed SS kick function to the one we extract from an exact numerical integration of Newton's equation for Halley's comet orbiting the SS constituted by the eight planets and the Sun (see snapshots in Fig. 1) from -1000 to +1000 Jovian years around J2000.0 ie from

---

*Email address:* jose.lages@utinam.cnrs.fr

(J. Lages)

*URL:* <http://perso.utinam.cnrs.fr/~lages>

(J. Lages)

about -10 000BC to about 14 000AD. Exact integration over a greater time interval does not provide exact ephemerides since Halley's comet dynamics is chaotic, see eg [6] where integration of the dynamics of SS constituted by the Sun, Jupiter and Saturn have been computed for  $10^6$  years.

## 2. Symplectic Halley map

Orbital elements of the current osculating orbit of 1P/Halley are [26]

$$\begin{aligned} e &\simeq 0.9671, & q &\simeq 0.586 \text{ au}, \\ i &\simeq 162.3, & \Omega &\simeq 58.42, \\ \omega &\simeq 111.3, & T_0 &\simeq 2446467.4 \text{ JD} \end{aligned}$$

Along this trajectory (Fig. 1) the comet's energy per unit of mass is  $E_0 = -1/2a = (e-1)/2q$  where  $a$  is the semi-major axis of the ellipse. In the following we set the gravitational constant  $G = 1$ , the total mass of the Solar system (SS) equal to 1, and the semi-major axis of Jupiter's trajectory equal to 1. In such units we have  $q \simeq 0.1127$ ,  $a \simeq 3.425$  and  $E_0 \simeq -0.146$ . Halley's comet pericenter can be written as  $q = a(1-e) \simeq \ell^2/2$  where  $\ell$  is the intensity per unit of mass of the comet angular momentum vector. Assuming that the latter changes sufficiently slowly in time we can consider the pericenter  $q$  as constant for many comet's passages through the SS. We have checked by direct integration of Newton's equations that this is actually the case ( $\Delta q \simeq 0.07$ ) at least for a period of -1000 to +1000 Jovian years around J2000.0. Consequently, Halley's comet orbit can be reasonably characterized by its semi-major axis  $a$  or equivalently by Halley's comet energy  $E$ . During each passage through the SS many body interactions with the Sun and the planets modify the comet's energy. The successive changes in energy characterize Halley's comet dynamics.

Let us rescale the energy  $w = -2E$  such as now positive energies ( $w > 0$ ) correspond to elliptic orbits and negative energies ( $w < 0$ ) to hyperbolic orbits. Let us characterize the  $n$ th passage at the pericenter by the phase  $x_n = t_n/T_J \bmod 1$  where  $t_n$  is the date of the passage and  $T_J$  is Jupiter's orbital period considered as constant. Hence,  $x$  represents an unique position of Jupiter on its own

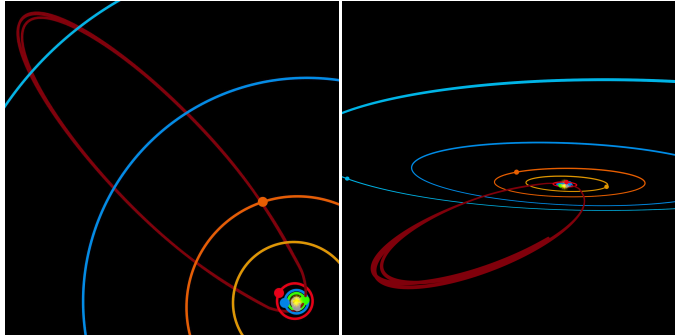


Figure 1: Two examples of three dimensional view of Halley's comet trajectory. The left panel presents an orthographic projection and the right panel presents an arbitrary point of view. The red trajectory shows three successive passages of Halley's comet through SS, the other near circular elliptic trajectories are for the eight Solar system planets, the yellow bright spot gives the Sun position. At this scale details of the Sun trajectory is not visible.

trajectory. The energy  $w_{n+1}$  of the osculating orbit after the  $n$ th pericenter passage is given by

$$\begin{aligned} w_{n+1} &= w_n + F(x_n) \\ x_{n+1} &= x_n + w_{n+1}^{-3/2} \end{aligned} \quad (1)$$

where  $F(x_n)$  is the kick function, *ie* the energy gained by the comet during the  $n$ th passage and depending on Jupiter phase  $x_n$  when the comet is at pericenter. The second row in (1) is the third Kepler's law giving the Jupiter's phase at the  $(n+1)$ th passage from the one at the  $n$ th passage and the energy of the  $(n+1)$ th osculating orbit.

The set of equations (1) is a symplectic map which captures in a simple manner the main features of Halley's comet dynamics. This map has already been used by Chirikov and Vecheslavov [1] to study Halley's comet dynamics from previously observed or computed perihelion passages from -1403BC to 1986AD[25]. In [1] Jupiter's and Saturn's contributions to the kick function  $F(x)$  had been extracted using Fourier analysis. In the next section we propose to semi-analytically compute the exact contributions of each of the eight SS planets and the Sun.

### 3. Solar system kick function

Let us assume a SS constituted by eight planets with masses  $\{\mu_i\}_{i=1,\dots,8}$  and the Sun with mass  $1 - \mu = 1 - \sum_{i=1}^8 \mu_i$ . The total mass of the SS is set to 1 and  $\mu \ll 1$ . In the barycentric reference frame we assume that the eight planets have nearly circular elliptical trajectories with semi-major axis  $a_i$ . We rank the planets such as  $a_1 < a_2 < \dots < a_8$  so  $a_5$  and  $\mu_5$  are the orbit semi-major axis and the mass of Jupiter. The corresponding mean planet velocities  $\{v_i\}_{i=1,\dots,8}$  are such as  $v_i^2 = \left(1 - \sum_{j \geq i} \mu_j\right) / a_i \simeq 1/a_i$ . Here we have set the gravitational constant  $G = 1$  and in the following we will take the mean velocity of Jupiter  $v_5 = 1$ . The Sun trajectory in the barycentric reference frame is such as  $(1 - \mu) \mathbf{r}_\odot = -\sum_{i=1}^8 \mu_i \mathbf{r}_i$ .

In the barycentric reference frame, the potential experienced by the comet is consequently

$$\begin{aligned} \Phi(\mathbf{r}) &= -\frac{1 - \mu}{\|\mathbf{r} - \mathbf{r}_\odot\|} - \sum_{i=1}^8 \frac{\mu_i}{\|\mathbf{r} - \mathbf{r}_i\|} \\ &= \Phi_0(r) \left[ 1 \right. \\ &\quad \left. + \sum_{i=1}^8 \mu_i \left( -1 - \frac{\mathbf{r} \cdot \mathbf{r}_i}{r^2} + \frac{r}{\|\mathbf{r} - \mathbf{r}_i\|} \right) \right] \\ &\quad + o(\mu^2) \end{aligned} \quad (2)$$

where  $\Phi_0(\mathbf{r}) = -1/r$  is the gravitational potential assuming all the mass is located at the barycenter.

Let us define a given osculating orbit  $\mathcal{C}_0$  with energy  $E_0$  and corresponding to the  $\Phi_0(r)$  potential. The change of energy for the comet following the osculating orbit  $\mathcal{C}_0$  under the influence of the SS potential  $\Phi(\mathbf{r})$  (2) is given by the integral

$$\Delta E(x_1, \dots, x_8) = \oint_{\mathcal{C}_0} \nabla (\Phi_0(r) - \Phi(\mathbf{r})) \cdot d\mathbf{r} \quad (3)$$

which gives at the first order in  $\mu$

$$\begin{aligned} &\Delta E(x_1, \dots, x_8) \\ &\simeq \sum_{i=1}^8 \mu_i \oint_{\mathcal{C}_0} \nabla \left( \frac{\mathbf{r} \cdot \mathbf{r}_i}{r^3} - \frac{1}{\|\mathbf{r} - \mathbf{r}_i\|} \right) \cdot d\mathbf{r} \quad (4) \\ &\simeq \sum_{i=1}^8 \Delta E_i(x_i) \end{aligned}$$

This change in energy depends on the phases ( $x_i = t/T_i \bmod 1$ ) of the planets when the comet passes through pericenter. From (4) we see that each planet contribution  $\Delta E_i(x_i)$  are decoupled from the others and can be computed separately.

The integral (3) is similar to the Melnikov integral (see eg [4, 20–24]) which is usually used in the vicinity of the separatrix to obtain the energy change of the pendulum perturbed by a periodic parametric term. In the case of the restricted 3-body problem the Melnikov integral can be used to obtain the energy change of the light body in the vicinity of 2-body parabolic orbit ( $w \simeq 0$ ) [4]. We checked that integration (3) along an elliptical osculating orbit or along the parabolic orbit corresponding to the same pericenter give no noticeable difference as long as the comet semi-major axis is greater than planet semi-major axis. To be more realistic we adopt integration over an elliptical osculating orbit  $\mathcal{C}_0$  since in the case of 1P/Halley slight differences start to appear for Neptune contribution to the kick function.

After the comet's passage at the pericenter, when the planet phases are  $x_1, \dots, x_8$ , the new osculating orbit corresponds to the energy  $E_0 + \Delta E(x_1, \dots, x_8)$ . Knowing the relative positions of the planets, the knowledge of eg  $x = x_5$  is sufficient to determine all the  $x_i$ 's. Hence, for Halley map (1) the kick function of the SS is  $F(x) = -2\Delta E(x) = \sum_{i=1}^8 F_i(x_i)$  where  $F_i(x_i)$  is the kick function of the  $i$ th planet. In the following we present results obtained from the computation of the Melnikov integral (3) using coplanar circular trajectories for planets. We have checked the results are quite the same in the case of the non coplanar nearly circular elliptic trajectories for the planets taken at J2000.0 (see dashed lines in Fig. 3 right panel).

Fig. 2 shows contributions for each of the eight planets to the SS kick function. The two uppermost panels in Fig. 2 right column show contributions of Jupiter,  $F_5(x)$ , and Saturn,  $F_6(x_6)$ , to the SS kick function. We set  $x = x_5 = 0$  when Halley's comet was at perihelion in 1986. We clearly see that the exact calculus of the Melnikov integral (3) are in agreement with the contributions of Jupiter and Saturn extracted by Fourier anal-

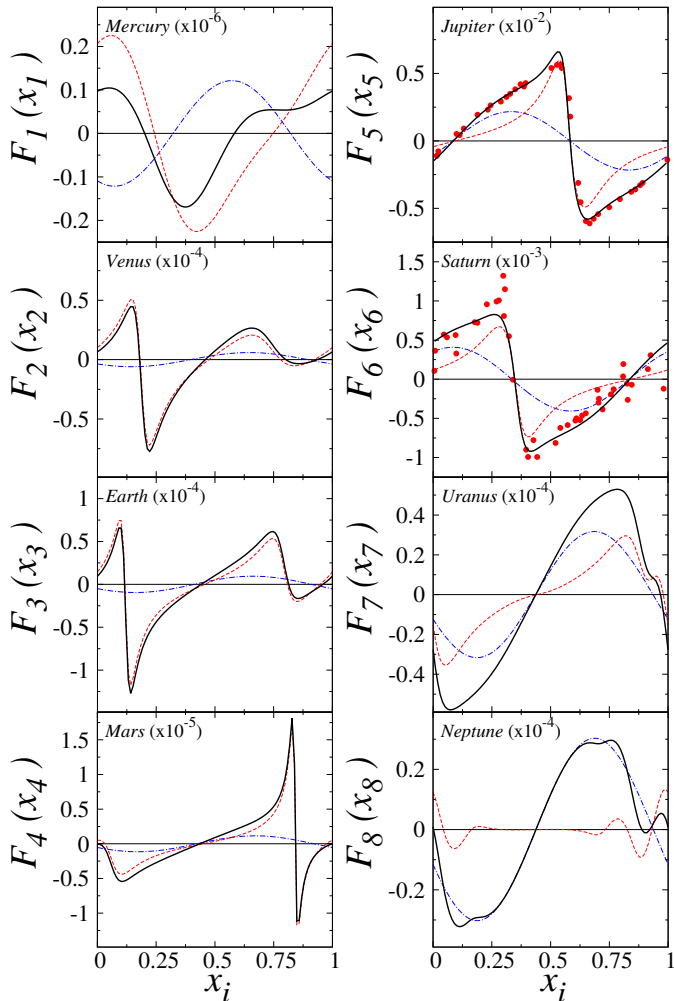


Figure 2: Contributions of the eight planets to SS kick function  $F(x)$ . On each panel  $F_i(x_i)$  is obtained from Melnikov integral calculation (thick line), the red dashed line (the blue dotted-dashed line) shows the Keplerian contribution (dipole contribution) to the Melnikov integral. On Jupiter and Saturn panels, the kick functions extracted by Fourier analysis from observations and exact numerical calculations are shown ( $\bullet$ , see Fig. 2 in [1]).

ysis [1] of previously observed and computed perihelion passages [25]. As seen in Fig. 2 the kick function is the sum of two terms (4): the Kepler potential term  $-\|\mathbf{r} - \mathbf{r}_i\|^{-1}$  (dashed red line in Fig. 2) and the dipole potential term  $\mathbf{r} \cdot \mathbf{r}_i/r^3$  (dot dashed blue line in Fig. 2). These two terms are of the same order of magnitude, the dipole term due to the Sun displacement around the SS barycenter is therefore not negligible for Jupiter (Saturn) kick function. The rotation of the Sun around SS barycenter creates a rotating circular

dipole of amplitude  $\mu_i \simeq M_i/M_S$  similar to the one analyzed for Rydberg molecular states [19] that gives additional kick function of sinus form.

In Fig. 2 we clearly see that the saw-tooth shape used in [1] to model the kick function is only a peculiar characteristic of Jupiter and Saturn contributions. Also, the sinus shape analytically found in [2] for large  $q$  can only be considered as a crude model for the planet contributions of the SS kick function. For Venus, Earth and Mars the kick function is dominated by the Kepler potential term, the dipole potential term being weaker by an order of magnitude. Uranus contribution to the SS kick function share the same characteristics as Jupiter's (Saturn's) contributions but two (one) orders of magnitude weaker. For Neptune as its semi-major axis is about 60 times greater than Halley's comet perihelion, the direct gravitational interaction of Neptune is negligible and the dipole term dominates the kick function. Neptune indirectly interacts on Halley's comet by influencing the Sun's trajectory. As Mercury semi-major axis is less than perihelion's comet, Mercury, like the Sun, acts as a second rotating dipole, consequently the two potential terms in (4) contribute equally.

For a given osculating orbit, the shape  $f_i(x_i)$  of the kick function defined such as  $F_i(x_i) = \mu_i f_i(x_i) v_i^2$  has to be only dependent on  $q/a_i$ . Let us use the case of 1P/Halley to study general features of  $f_i(x_i)$ . Fig. 3 left panel shows the peak amplitude  $f_{i,max}$  of  $f_i(x_i)$ . In the region  $0.25 \lesssim q/a_i \lesssim 0.75$  the peak amplitude  $f_{i,max}$  is clearly dominated by the Keplerian potential term and even diverges for close encounters at  $q \simeq 0.3a_i$  and  $q \simeq 0.7a_i$ . For  $q \gtrsim 1.5a_i$  the Keplerian potential and the circular dipole potential terms give comparable sine waves almost in phase opposition (Fig.2 top left panel and [27]). We clearly observe for  $q \gtrsim 1.5a_i$  an exponential decrease of the peak amplitude,  $f_{i,max} \sim \exp(-2.7q/a_i)$ , consistent with the two dimensional case studied in [2, 3].

The orbital frequency of the planets being only near integer ratio, for a sufficiently long time randomization occurs and any 8-tuple  $\{x_i\}_{i=1,\dots,8}$  can represent the planets position in the SS. For

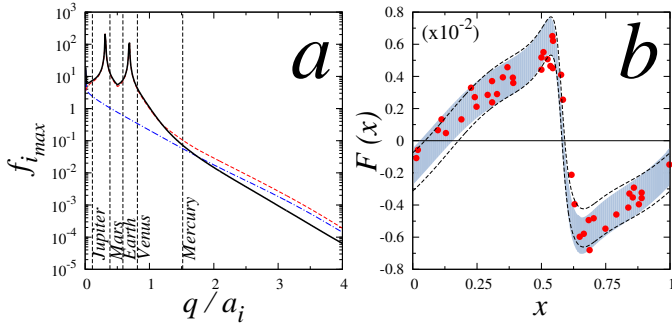


Figure 3: Left panel: Peak amplitude of the kick function shape  $f_i(x_i)$  (thick black line) as a function of pericenter distance  $q/a_i$  [27]. The red dashed line (the blue dotted-dashed line) shows the maximum amplitude of the Keplerian contribution (dipole contribution). Vertical dashed lines show relative positions of planets. On that scale Saturn, Uranus and Neptune relative positions are not shown. Right panel: Variation domain of the SS kick function  $F(x)$  (light blue shaded area) as a function of Jupiter's phase  $x = x_5$ . The variation width is  $\Delta F \simeq 0.00227$ . Data from observations and exact numerical calculations (Fig. 1 from [1]) are shown ( $\bullet$ ). The dashed lines bound the variation domain of the SS kick function when current elliptical trajectories for planets are considered.

$x = x_5$  the SS kick function  $F(x)$  is a multivalued function for all  $0 \leq x \leq 1$ . We can nevertheless define a lower and upper bound to the SS kick function which are presented as the boundaries of the blue shaded region in Fig. 3 right panel. We clearly see that raw data points extracted in [1] from previously observed and computed Halley's comet passages at perihelion [25] lie in the variation domain of  $F(x)$  deduced from the Melnikov integral (3).

#### 4. Chaotic dynamics of Halley's comet

The main contribution to the SS kick function  $F(x)$  is  $F_5(x)$  the one from Jupiter as the other planet contributions are from 1 (Saturn) to 4 (Mercury) orders of magnitude weaker. The dynamics of Halley's comet is essentially governed by Jupiter's rotation around the SS barycenter. The red shaded area on Fig. 4 shows the section of Poincaré obtained from Halley map (1) taking only into account Jupiter's contribution  $F(x) = F_5(x)$ . We clearly see that the accessible part of the phase space is densely filled which

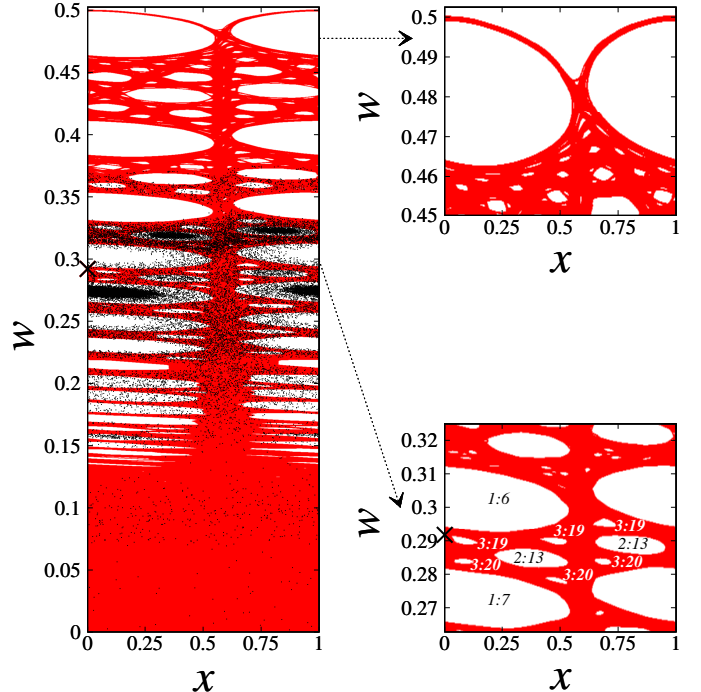


Figure 4: Left panel: Poincaré section of Halley's map generated only by Jupiter's kick contribution  $F_5(x)$  (red area). The cross symbol ( $\times$ ) at  $(x = 0, w \simeq 0.2921)$  gives Halley's comet state at its last 1986 perihelion passage. An example of orbit generated by the Halley map (1) with the contributions of all the planets is shown by black dots. Right top panel: closeup on the invariant KAM curve stopping chaotic diffusion. Right bottom panel: closeup centered on Halley's current location. Stability islands are tagged with the corresponding resonance  $p:n$  between Halley's comet and Jupiter orbital movements.

is a feature of dynamical chaos. In the region  $0 < w \lesssim w_{cr} \simeq 0.125$  the comet can rapidly diffuses through a chaotic sea whereas in the sticky region  $w_{cr} \simeq 0.125 \lesssim w \lesssim 0.5$  the diffusion is slowed down by islands of stability. The estimated threshold  $w_{cr} \simeq 0.125$  is the same as the one estimated analytically in the saw-tooth shape approximation in [1]. Stability islands are located far from the separatrix ( $w = 0$ ) on energies corresponding to resonances with Jupiter. The current position of Halley's comet ( $x = 0, w \simeq 0.2921$ ) is between two stability islands associated with 1:6 and 3:19 resonances with Jupiter orbital movement (Fig. 4 right bottom panel). As the comet's dynamics is chaotic the unavoidable imprecision on the current comet energy  $w$  allows us only to follow its trajectory in a statistical sense. Ac-

according to the Poincaré section (Fig. 4) associated with Halley map (1) for  $F = F_5$  the motion of the comet is constrained by a KAM invariant curve around  $w \simeq 0.5$  (Fig. 4 top right panel) constituting an upper bound to the chaotic diffusion. Consequently as the comet dynamics is bounded upwards the comet will be ejected outside SS as soon as  $w$  reaches a negative value. Taking  $10^5$  random initial conditions in an elliptically shaped area with semi-major axis  $\Delta x = 5 \cdot 10^{-3}$  and  $\Delta w = 5 \cdot 10^{-5}$  centered at the current Halley's comet position ( $x = 0, w = 0.2921$ ) we find a mean sojourn time of  $\bar{\tau} \simeq 4 \cdot 10^8$  yr and a mean number of kicks of  $\bar{N} \simeq 4 \cdot 10^4$ . A wide dispersion has been observed since  $3 \cdot 10^5$  yr  $\lesssim \tau \lesssim 3 \cdot 10^{13}$  yr and  $749 \leq N \lesssim 9 \cdot 10^7$ .

Now let us turn on also the other planets contributions. As shown in [6], where only Jupiter and Saturn are considered, diffusion inside previously depicted stability islands is now allowed as the other planets act as a perturbation on the Jupiter's kick contribution. In the example presented in Fig. 4 left panel the comet is locked for a huge number of successive kicks in a 1:7 and 2:11 resonances with Jupiter around  $w \simeq 0.27$  and  $w \simeq 0.32$ . We have also checked that for some other initial conditions even close to the previous example one the KAM invariant curve around  $w \simeq 0.5$  associated with the Jupiter contribution (see Fig. 4 top right panel) no more stops the diffusion towards  $w \sim 1$  region where the kicked picture and therefore the map description are no more valid. Taking statistically the same conditions as in the only Jupiter contribution case we discard about 11% of the initial conditions giving orbits exploring the region  $w > 0.5$  and for the remaining initial conditions we obtain a mean sojourn time of  $\bar{\tau}' \simeq 4 \cdot 10^7$  yr and a mean number of kicks of  $\bar{N}' \simeq 3 \cdot 10^4$ . A wide dispersion has been observed since  $1 \cdot 10^5$  yr  $\lesssim \tau' \lesssim 6 \cdot 10^{11}$  yr and  $559 \leq N' \lesssim 5 \cdot 10^5$ . The two maps give comparable mean number of kicks  $\bar{N}' \sim \bar{N}$  but the mean sojourn time is ten time less in the case of the all-planets Halley map ( $\bar{\tau} \sim 10 \bar{\tau}'$ ). This is due to the fact that the comet can be locked in for a great number of kicks in Jupiter resonances at large  $0.5 \gtrsim w \gtrsim 0.125$  which correspond to small

orbital periods. In accordance with the results presented in [1] we retrieve for the mean sojourn time a 10 factor between the only Jupiter contribution case and the all planets contribution case (Jupiter and Saturn only in [1]). But we note that the mean sojourn times computed here are 10 times greater than those computed in [1] where only 40 initial conditions have been used.

## 5. Robustness of the symplectic map description

In order to test the robustness of the kicked picture for Halley's comet dynamics we have directly integrated Newton's equations for a period of -1000 to +1000 Jovian years around J2000.0 in the case of a SS constituted by the Sun and the eight planets with coplanar circular orbits (Fig. 5 first row), the Sun and Jupiter with elliptical orbits (Fig. 5 second row), and the Sun and the eight planets with elliptical orbits (Fig. 5 third row). From Fig. 5 right panels we see that our modern era is embedded in a time interval  $-400P_J < t < 200P_J$  ( $-2800\text{BC} < t < 4400\text{AD}$ ) with quite constant Halley's comet energy  $w \simeq 0.29$  and perihelion  $q \simeq 0.11$ . This relatively dynamically quiet time interval allows the good agreement between our semi-analytic determination of SS kick function using the Melnikov integral (3) and the SS kick function extracted [1] from previously observed and computed perihelion passages [25].

In Fig. 5 left panels we reconstruct as in [1] the kick function using the dates  $t_n$  of the Halley's comet passages at perihelion  $F(x_n) = (t_{n+1} - t_n)^{-2/3} - (t_n - t_{n-1})^{-2/3}$ . We clearly see that these kick function values lie in the variation domain of the SS kick function when coplanar circular orbits are considered for the Sun and the planets (Fig. 5a). In the case of non coplanar elliptical orbits (Fig. 5c and e) the agreement is good but weaker than the coplanar circular case. This is due to Halley's comet precession which introduces a phase shift in  $x$  (see gradient from black to green color in Fig. 5a, c and e). As the coplanar circular orbits case possesses an obvious rotational symmetry, it is much less affected by the comet precession (Fig. 5a).

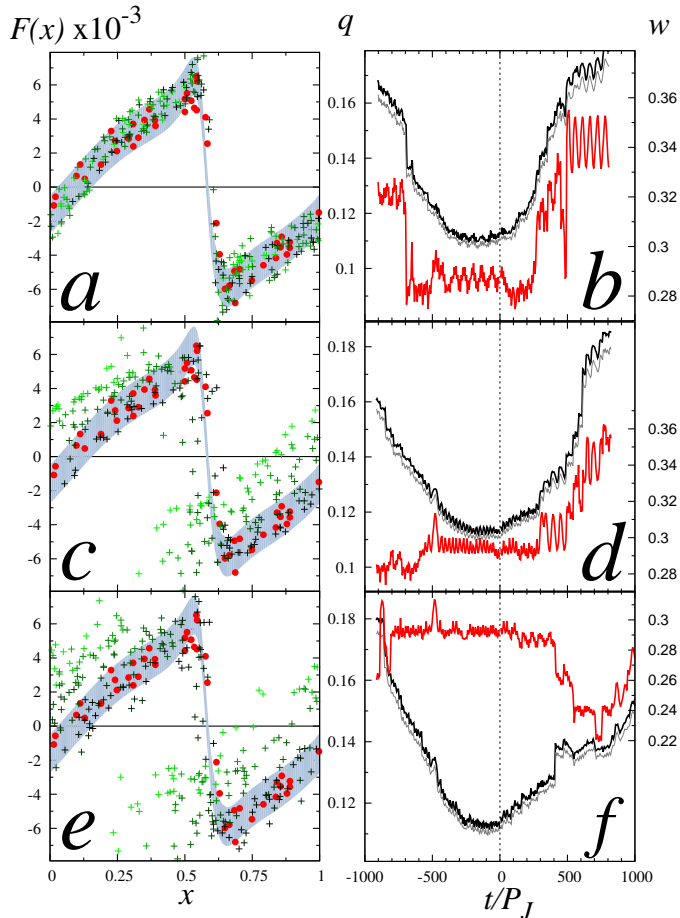


Figure 5: Numerical simulation of Halley’s comet dynamics over a time period of  $-1000$  to  $1000$  Jovian years around J2000.0 ( $t = 0$ ) with SS modeled as (a, b) the Sun and 8 planets with coplanar circular orbits, (c, d) the Sun and Jupiter with non coplanar elliptical orbits, (e, f) the Sun and the eight planets with non coplanar elliptical orbits. Left panels: kick function  $F(x)$  values (+) extracted from 290 successive simulated pericenter passages of Halley’s comet. The color symbol goes linearly from black for data extracted at time  $t = 0$  to light green for data extracted at time  $|t| \simeq 10^3 P_J$ . We show only points in the range  $-0.008 < F(x) < 0.008$ . Data from observations and exact numerical calculations (Fig. 1 from [1]) are shown ( $\bullet$ ). Right panels: time evolution of pericenter  $q$  (black curves, left axis) and of the osculating orbit energy  $w$  (red curves, right axis). Numerical simulations have been done time forward and time backwards from  $t = 0$ . The gray curves show the time evolution of the  $\ell^2/2$  quantity.

In Fig. 5 left panels we show only kick function values in the interval range  $-0.008 < w < 0.008$  corresponding to the variation range of the SS kick function (Fig. 3 right panel) obtained using

Melnikov integral (3). Around the sharp variation  $x \simeq 0.6$  we obtained few kick function values outside this energy interval (up to  $|F| \simeq 0.05$ ) which corresponds to big jumps in energy (eg at  $t \simeq 400 P_J$  in Fig. 5f) shown in Fig. 5 right panels. We have checked that those big jumps occur when Halley’s comet at its perihelion approaches closer to Jupiter. As a consequence the two dimensional Halley map (1) can be used with confidence only for short intervals of time  $\Delta t \lesssim 10^4$ yr such as eg the one at  $-400 P_J \lesssim t \lesssim 200 P_J$  in Fig. 5 right panels.

## 6. Conclusion

We have exactly computed the energy transfer from the SS to 1P/Halley and we have derived the corresponding symplectic map which characterizes 1P/Halley chaotic dynamics. With the use of Melnikov integral, energy transfer contributions from each SS planets have been isolated. In particular, we have retrieved the kick functions of Jupiter and Saturn previously extracted by Fourier analysis [1]. The Sun movement around SS barycenter induces a rotating gravitational dipole potential which is non negligible in the energy transfer from the SS to 1P/Halley. The symplectic Halley map allows us to follow the chaotic trajectory of the comet during relatively quiet dynamical periods  $\Delta t \lesssim 10^4$ yr exempt of closer approach with major planets. One can expect that a higher dimensional symplectic map involving the angular momentum and other orbital elements would allow to follow Halley’s comet dynamics for longer periods taking into account large variation in energy (close planet approach) and precession. In spite of the slow time variation of the Halley map parameters such a symplectic map description allows to get a physical understanding of the global properties of comet dynamics giving a local structure of phase space and a diffusive time scale of chaotic escape of the comet from the Solar system.

## Acknowledgments

The authors thank D. L. Shepelyansky for useful comments on the current work.

## References

- [1] B. V. Chirikov and V. V. Vechev, *Chaotic dynamics of comet Halley*, A&A 221, 146-154 (1989)
- [2] T. Y. Petrosky, *Chaos and cometary clouds in the solar system*, Phys. Lett. A 117, 328-332 (1986)
- [3] T. Y. Petrosky and R. Broucke, *Area-preserving mappings and deterministic chaos for nearly parabolic motions*, Celest. Mech. Dyn. Astron. 42, 53 (1988)
- [4] J. Liu and Y. S. Sun, *Chaotic motion of comets in near-parabolic orbit: Mapping approaches*, Celest. Mech. Dyn. Astron. 60, 3 (1994)
- [5] I. I. Shevchenko, *The Kepler map in the three-body problem*, New Astronomy 16, 9499 (2011)
- [6] R. Dvorak and J. Kribbel, *Dynamics of Halley-like comets for 1 million years*, A&A 227, 264-270 (1990)
- [7] L. Mal'ushkin and S. Tremaine, *The Keplerian Map for the Planar Restricted Three-Body Problem as a Model of Comet Evolution*, Icarus 142, 341 (1999)
- [8] M. Pan and R. Sari, *A generalization of the Lagrangian points: studies of resonance for highly eccentric orbits*, Astron. J. 128, 1418 (2004)
- [9] V. V. Emelyanenko, *Dynamics of periodic comets and meteor streams*, Celest. Mech. Dyn. Astron. 54, 91 (1992)
- [10] J. L. Zhou, Y. S. Sun, J. Q. Zheng, and M. J. Valtonen, *The transfer of comets from near-parabolic to short-period orbits: map approach*, Astron. Astrophys. 364, 887 (2000)
- [11] J. L. Zhou and Y. S. Sun, *Lévy flights in comet motion and related chaotic systems*, Phys. Lett. A 287, 217 (2001)
- [12] J. L. Zhou, Y. S. Sun, and L. Y. Zhou, *Evidence for Lévy random walks in the evolution of comets from the Oort cloud*, Celest. Mech. Dyn. Astron. 84, 409 (2002)
- [13] I. B. Khriplovich and D. L. Shepelyansky, *Capture of dark matter by the Solar System*, Int. J. Mod. Phys. D 18, 1903 (2009)
- [14] J. Lages and D. L. Shepelyansky, *Dark matter chaos in the Solar System*, MNRAS 430, L25-L29 (2013)
- [15] G. Rollin, J. Lages, and D. L. Shepelyansky, *Chaotic enhancement of dark matter density in binary systems and galaxies*, arXiv:1403.0254
- [16] G. Casati, I. Guarneri, and D. L. Shepelyansky, *Exponential photonic localization for hydrogen atom in a monochromatic field*, Phys. Rev. A 36, 3501 (1987)
- [17] G. Casati, I. Guarneri, and D. L. Shepelyansky, *Classical chaos, quantum localization and fluctuations: a unified view*, Physica A 163, 205 (1990)
- [18] D. L. Shepelyansky, *Microwave ionization of hydrogen atoms*, Scholarpedia 7(1), 9795 (2012)
- [19] F. Benvenuto, G. Casati, and D. L. Shepelyansky, *Chaotic autoionization of molecular Rydberg states*, Phys. Rev. Lett. 72, 1818-1821 (1994)
- [20] B. V. Chirikov, *A Universal Instability of Many-Dimensional Oscillator Systems*, Phys. Rep. 52, 264-379 (1979)
- [21] G. M. Zaslavsky, *Physics of Chaos in Hamiltonian Dynamics*, Imperial College Press, London (1998)
- [22] G. M. Zaslavsky, *Hamiltonian Chaos and Fractional Dynamics*, Oxford University Press, Oxford (2005)
- [23] L. Reichl, *The Transition to Chaos*, 2nd edition, Springer-Verlag, New York (2004)
- [24] V. Afraimovich and S.-B. Hsu, *Lectures on Chaotic Dynamical Systems*, American Mathematical Society, International Press (2003)
- [25] D. K. Yeomans and T. Kiang, *The long-term motion of comet Halley*, MNRAS 197, 633-646 (1981)
- [26] NASA JPL HORIZONS Solar System Dynamics <http://ssd.jpl.nasa.gov>
- [27] Supplementary material is available at <http://perso.utinam.cnrs.fr/~lages/publications/sm/sm21.html>



This figure "sm21\_still.png" is available in "png" format from:

<http://arxiv.org/ps/1410.3727v2>